EXPERIMENTAL CONFIRMATION OF LIMIT CYCLE OSCILLATION FOR ACTIVE CONTROL OF TRANSONIC FLUTTER IN WIND TUNNEL

Hiroshi Matsushita*, Jun Hatta, and Kenichi Saitoh*****
***University of Fukui, **Brother Industries, Ltd., and ***JAXA, Japan**

Keywords: *Transonic Flutter, Active Flutter Control, Limit Cycle Oscillation, Bifurcation*

Abstract

The wind tunnel test was carried out with great care obtaining successfully limited numbers of LCO data at dynamic pressures above the open loop flutter point. After confirming a flutter dynamic pressure of the controlled wing, we tried to excite the wing by a leading edge control surface oscillation at three different dynamic pressures in between the open and the closed loop flutter dynamic pressure. Even though the control might have lost the effectiveness due to large amplitude of LCO and resulting amplitude might have broken the wing seriously, we have succeeded in getting smaller amplitude of LCO. Adjusting the mathematical model to new wind tunnel test data, the model could predict the closed loop bifurcation that shows good correspondence to the test data.

1 Introduction

In transonic regions, flutter often takes the form of a limit cycle oscillation (LCO) caused by the nonlinear behavior of the transonic aerodynamics due to a shock wave moving on the wing surface coupled with the flow separation [1]-[3]. The present authors have developed a nonlinear mathematical model that can explain the most of the bifurcation characteristics observed in the series of transonic wind tunnel tests executed at the National Aerospace Laboratory in Japan (NAL, now Japan Aerospace Exploration Agency (JAXA)) for a high aspect ratio wing model [4].

An efficient method to increase the flutter velocity in the transonic region may contribute greatly to aircraft performance because in this region there is a phenomenon known as a transonic dip where the flutter velocity drops significantly against a flight Mach number [5]. Active control technology of flutter is one of the most promising technologies that enable to increase the flutter velocity without performance penalty. The present authors proposed a practical control law design method that produces a robust controller against the model uncertainty [6].

Bifurcation diagram of transonic flutter, either observed in the wind tunnel tests or predicted by the mathematical model, is classified as a subcritical Hopf bifurcation type, which means that the LCO type flutter may occur at lower dynamic pressure than the nominal flutter, by more than 10 % [7].

The present authors also developed the analytical method for the closed loop bifurcation characteristics using a continuation method [7]. However, we didn't have any experimental data that confirm the analytical prediction of the bifurcation diagram. We then have made planning to add one more wind tunnel test at the transonic wind tunnel at JAXA on April 2005.

2 Limit Cycle Oscillations and Bifurcation for Transonic Flutter Observed in Wind Tunnel Tests

Figure 1 shows a wind tunnel model of a high aspect ratio wing. It has a leading edge- and a trailing edge-control surface (shown as hatching parts). They are used for active flutter control research [6]. The wing has an enlarged middle part where two sets of electric motors for control are installed. For LCO investigation

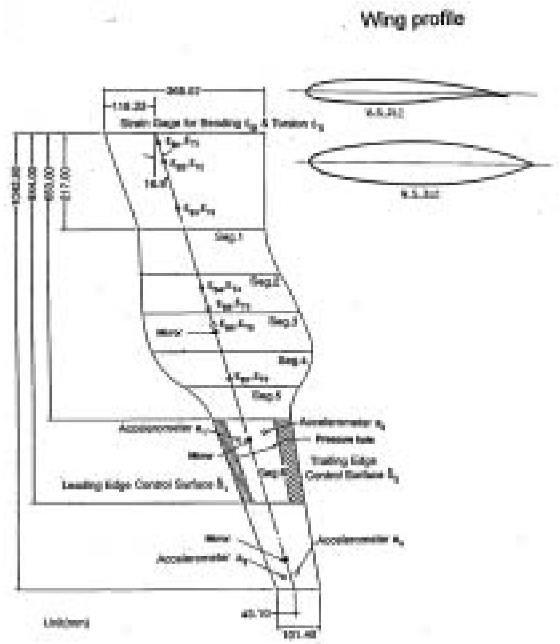

Fig. 1 High aspect ratio wing model

in the wind tunnel tests, a leading edge control surface is used as a source of excitation and wing response is measured by four accelerometers and seven sets of torsion and bending strain gages, which are fixed along an aluminum spar of the wing.

In the series of wind tunnel experiments at the transonic wind tunnel of the National Aerospace Laboratory in Japan, it was turned out that this wing behaves a typical transonic flutter. The wing has a minimum dynamic pressure at a transonic region (known as transonic dip phenomena) and every flutter has

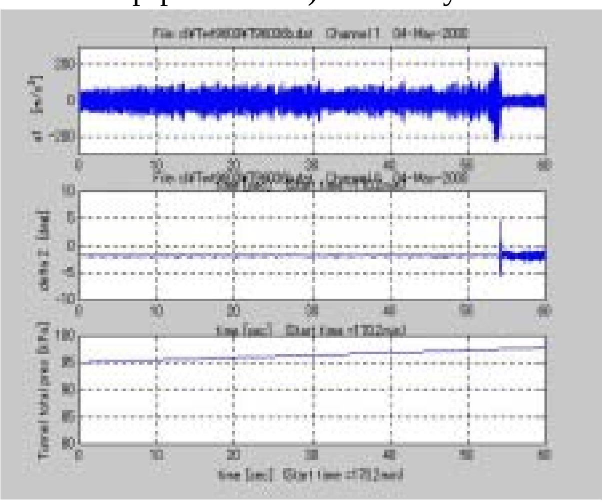

Fig. 2 Time history of nominal flutter occurrence during the increase of the wind tunnel pressure.

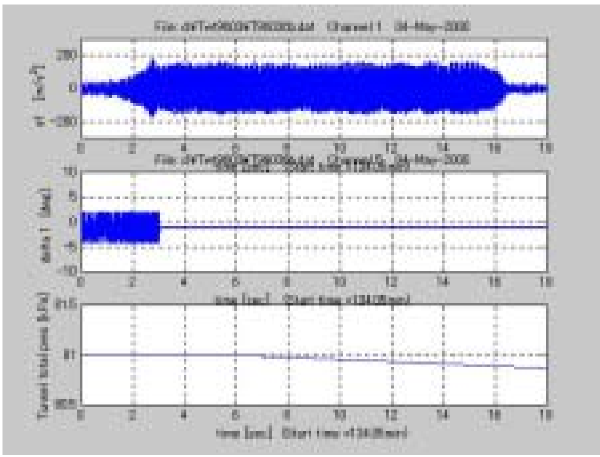

Fig. 3 Quasi-steady decrease of the dynamic pressure at the saddle-node bifurcation

the form of LCO. In each flutter, when the tunnel pressure is increased as shown at the bottom time chart in Fig. 2 as a typical case of Mach 0.8, the wing jumps up to LCO at a specified (nominal) dynamic pressure as shown at the top chart in the figure. (Since this figure shows the active flutter test result [6], the LCO flutter is stopped right after its occurrence by activating a trailing edge control surface as shown at the middle chart.) Successive investigation cleared that, even at lower dynamic pressure than the nominal pressure stated above, the wing can be brought into LCO state if it's excited above a certain energy level. Once LCO state is attained, it is kept continuing even after removing the excitation. LCO thus attained is stabilized again if the tunnel pressure is further decreased. These phenomena are presented in Fig. 3 where the LCO is established by a leading edge excitation as shown at the middle chart in this case, and continues to oscillate even after removing the excitation. Then LCO continues to oscillate during the quasi-steady decrease of the wind tunnel pressure until it ceases to rest at a certain value of the pressure. That point corresponds to a saddle-node bifurcation.

Figure 4 summarizes these phenomena found in the tests as a bifurcation diagram where the LCO amplitude is depicted against the dynamic pressure. In this figure the stability boundary, or unstable limit cycle expressed by the crosses, has a deviation and the stable region

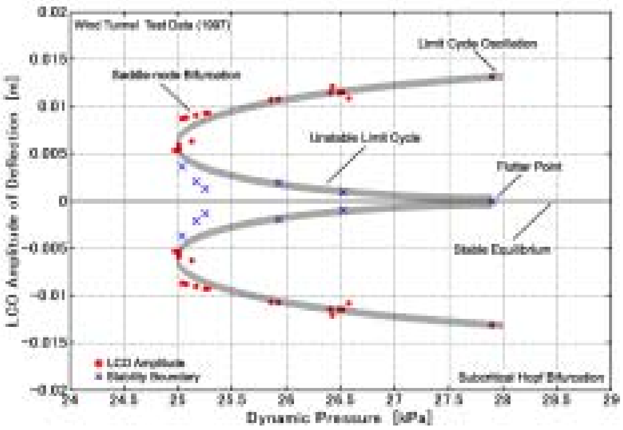

Fig. 4 Bifurcation diagram obtained from 1997 wind tunnel test

under the boundary is rather narrow. Disturbances around the wing such as turbulence in the wind tunnel flow, the flow separation occurred at the wing surface, etc., may decrease the stable region in the experimentally obtained diagram.

$$x(t) = \left[q(t)^T \quad \delta_2(t) \quad \dot{q}(t)^T \quad \dot{\delta}_2(t) \quad r(t)^T \right]^T \in R^{14\times 1}$$

3 Nonlinear Mathematical Model for Transonic Flutter and Open Loop Bifurcation

The authors *et al.* have developed a nonlinear mathematical model in the form of 2-DOF, finite state nonlinear differential equation introducing the fourth order nonlinearity to the generalized aerodynamic damping terms [8]. Extending to four modes, we have obtained the following 14th order nonlinear differential equation, with a system noise $w(t)$ included,

$$\begin{aligned} &\dot{x} = Ax + \Delta A_{NL} x + Bu + Gw(t); \\ &x = \left[q^T \quad \delta_2 \quad \dot{q}^T \quad \dot{\delta}_2 \quad r^T \right]^T \in R^{14\times 1} \\ &u = \delta_2 \end{aligned} \qquad (1)$$

where q is the generalized coordinates and r is the augmented variable expressing the unsteady aerodynamic delay. A, B, G are linear and ordinary part of the system matrices for flutter analysis as shown below.

$$A = \begin{bmatrix} 0 & 0 & I_4 & 0 & 0 \\ 0 & 0 & 0 & I_1 & 0 \\ A_1 & A_2 & A_3 & A_4 & A_5 \\ 0 & -K_\delta & 0 & -C_\delta & 0 \\ B_{0q} & B_{0\delta} & 0 & 0 & \Lambda \end{bmatrix} \in R^{14\times 14} \qquad (2a)$$

$$B = \begin{bmatrix} 0 \\ -M_q S_\delta K_\delta \\ K_\delta \\ 0 \end{bmatrix} \in R^{14\times 1} \qquad (2b)$$

$$G = \begin{bmatrix} 0 \\ I_5 \\ 0 \end{bmatrix} \in R^{14\times 5} \qquad (2c)$$

where,

$$\begin{aligned} &A_1 = -M_q (K - A_{2q}),, \ A_2 = M_q \{ S_\delta K_\delta + A_{2\delta} \} \\ &A_3 = -M_q (B_c - A_{1q}), \ A_4 = M_q \{ S_\delta C_\delta + A_{1\delta} \} \\ &A_5 = M_q \end{aligned} \qquad (3)$$

and

$$\begin{aligned} M_q &= (M - A_{0q})^{-1} \\ S_\delta &= (S - A_{0\delta}) \end{aligned} \qquad (4)$$

In the above equations, M, C, and K are mass, structural damping, and stiffness matrices, respectively, while A_2, A_1, A_0, B_0 and Λ comprise the finite state aerodynamic model. The matrix ΔA_{NL} in eq. (1) represents a nonlinear terms and has the following form.

$$\Delta A_{NL} = \begin{bmatrix} 0 & 0 & 0 & 0 & 0 \\ 0 & 0 & 0 & 0 & 0 \\ 0 & 0 & M_q A_{1q} \Delta A_{INL} & 0 & 0 \\ 0 & 0 & 0 & 0 & 0 \\ 0 & 0 & 0 & 0 & 0 \end{bmatrix} \in R^{14\times 14} \qquad (5)$$

$$\Delta A_{INL} = \begin{bmatrix} (\beta \dot{q}_1^2 + \gamma \dot{q}_1^4) & 0 & 0 & 0 \\ 0 & 0 & 0 & 0 \\ 0 & 0 & 0 & 0 \\ 0 & 0 & 0 & 0 \end{bmatrix} \in R^{4\times 4} \qquad (6)$$

where (1, 1) element is the aerodynamic damping coefficients for bending deflection.

In order to make comparison of the mathematical model with the test results, an output equation that relates the state variables in Eq. (1) with the output variables measured in the wind tunnel tests is necessary. Since two sets of measured and derived variables, acceleration a_1, a_2, velocity v_1, v_2 and deflection d_1, d_2 at two accelerometer positions on the wing are enough for comparison, the output equation will take the form, with $v(t)$ denoting a measurement noise,

$$y = Cx + Du + v(t)$$
$$y = [a_1, a_2, v_1, v_2, d_1, d_2]^T \in R^6 \tag{7}$$

As for the two coefficients, C and D in the above equation, reader can refer Ref. [10]. A set of equations (1) and (7) comprises the nonlinear mathematical model for transonic flutter.

Christiansen and Lehn-Schiøler have applied the continuation method to the nonlinear mathematical model of Ref. [8] modifying a computer program package of the method [11 - 12]. The package features a fourth order Runge-Kutta integrator with fixed size which is capable of making analysis of limit cycles using Poincaré sections as the control parameter (dynamic pressure in the present case) is continuously changing. The continuation method can thus trace continuously the Poincaré section, even through the unstable limit cycle branch, once at the initial stage LCO amplitude

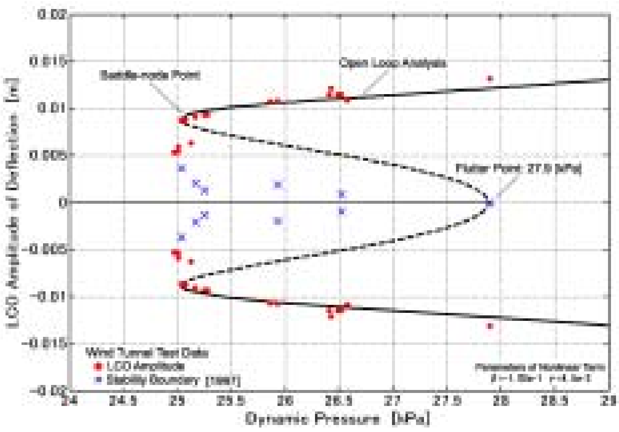

Fig. 5 Analytical bifurcation diagram based on 1997 wind tunnel test

has been captured. They could obtain the smooth curve in the bifurcation diagram.

Making use of the continuation method for the optimum combination of parameters, we have reached the values of β = -1.05e-1 and γ = 4.5e-3. Resulting bifurcation diagram is shown as a solid line in Fig. 5. In the figure experimental data are also plotted. The correspondence of the LCO between the math model and the experiment is quite good; the amplitude of LCO is almost identical and the position of the saddle-node bifurcation is exactly the same. There still remains a difference in unstable limit cycle; the mathematical model has a wide stable area under the unstable limit cycle, while the experimental data shows a limited region of stability. As stated earlier, the main reason of this discrepancy may exist in the noise effects. In real situation, even at the stable region disturbance may energize the wing to jump up to unstable region and push the wing to LCO state.

4 Robust Controller for Flutter Suppression and Closed Loop Bifurcation Diagram

4.1 Robust Controller Design

Robust stability control design based on left coprime factors approach [13] was applied to this wing model and the reduced order controller was obtained by the residualization method yielding control laws with a certain level of robustness [13].

With the expression of the nominal plant model $P(s)$ in a normalized left coprime factorisation,

$$P(s) = (A, B, C, D) = M(s)^{-1} N(s) \tag{8}$$

the uncertainties in the plant can be represented in terms of additive stable perturbations Δ_M, Δ_N to the factors in a coprime factorization of the plant as,

$$\tilde{P} = (M + \Delta_M)^{-1} (N + \Delta_N) \tag{9}$$

With the positive definite solutions X, Y of the algebraic Riccati solutions, a maximum stability margin $\varepsilon_{\max}$ is given by,

$$\varepsilon_{\max} = \left(1 + \lambda_{\max}(XY)\right)^{-1/2} \tag{10}$$

where $\lambda_{\max}(XY)$ is a Hankel norm. Choosing the stability margin ε such that $0 < \varepsilon < \varepsilon_{\max}$, the state space realization of a central controller $K_I(s)$ can explicitly be given, using Doyle's notation, as

$$K_I = \left[\begin{array}{c|c} \mathbf{A_a} - \mathbf{B_a B_a}^{\mathbf{T}}\mathbf{X} + \varepsilon^{-2}\mathbf{W}_r^{-\mathbf{T}}\mathbf{YC_a}^{\mathbf{T}}\mathbf{C_a} & \varepsilon^{-2}\,\mathbf{W}_r^{-\mathbf{T}}\mathbf{YC_a}^{\mathbf{T}} \\ \mathbf{B_a}^{\mathbf{T}}\mathbf{X} & 0 \end{array}\right] \tag{11}$$

where

$$W_r = \left(1 - \varepsilon^{-2}\right)I + XY \tag{12}$$

Controller given by eq. (11) has the same order to the mathematical model of the flutter and should be reduced in order. Making residualization for order reduction, we have obtained reduced eighth order controller as in the following form.

$$\begin{aligned} \dot{z} &= Fz + Gy \\ u &= Hz + Jy \end{aligned} \tag{13}$$

This controller was designated as CT03-161 and was used in the transonic wind tunnel testing carried out at NAL and attained 10.9% increase of flutter speed [6]. The Bode diagram of the controller is in Fig. 6.

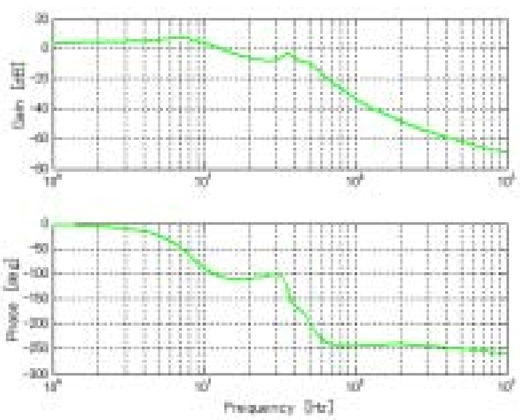

Fig. 6 Bode diagram of controller CT03-161

Besides the controller, we use an anti-aliasing filter to prevent a possible aliasing in sampling analog signal and include a model for A/D converter. These model can be expressed by the following two equations, respectively.

$$\dot{y}_1 = \omega_f y_1 - \omega_f y \tag{14}$$

$$\dot{y}_2 = -f_d y_2 - \dot{y}_1 + f_d y_1 \tag{15}$$

In these equations, acceleration output y produces filter output y_1, which in turn produces the converter output y_2.

4.2 Closed Loop Bifurcation Diagram

The procedure of bifurcation analysis for a closed loop system can be developed using a continuation method. Substituting the control law (13) into the state equation (1) with the output equation (7) along with an anti-aliasing filter and a model of A/D converter, we can obtain the following homogeneous equation for closed loop system,

$$\begin{bmatrix} \dot{x}(t) \\ \dot{\hat{x}}(t) \end{bmatrix} = \tilde{A}o \begin{bmatrix} x(t) \\ \hat{x}(t) \end{bmatrix} \tag{14}$$

where the system matrix is

$$\tilde{A}o = \begin{bmatrix} A + \Delta A_{NL} & -BK_1 \\ K_2 C(\bar{q}) & A_F(\bar{q}) \end{bmatrix} \in R^{28\times 28} \tag{15}$$

$A_F(\bar{q}) = A(\bar{q}) - B(\bar{q})K_1 - K_2 C(\bar{q})$. The coefficients $A(\bar{q})$ $B(\bar{q})$ $C(\bar{q})$ are evaluated at a

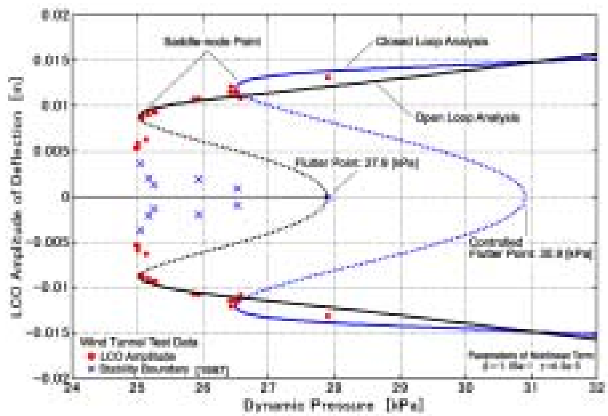

Fig. 7 Closed loop bifurcation diagram compared with open loop

Fig. 8 Model installed in the wind tunnel test section

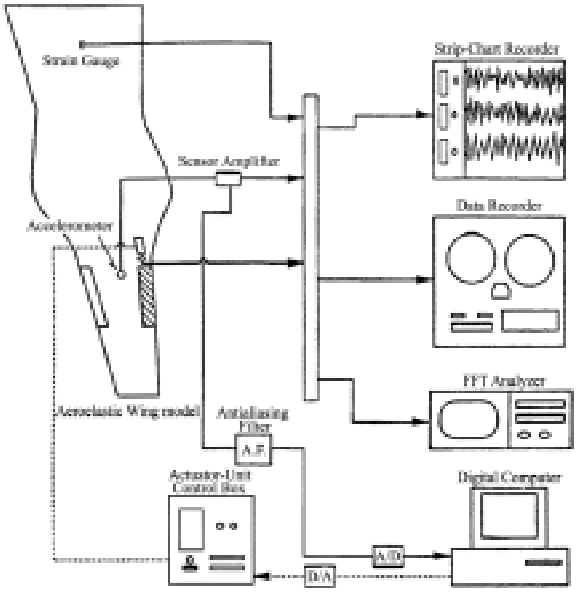

Fig. 9 Wind tunnel instrumentation for flutter control.

design dynamic pressure $\bar{q}$. Now a continuation method can be applied as in an open loop system. Figure 7 shows the analytical results for closed loop bifurcation diagram obtained by Eq. (14) by continuation method. In the figure, open loop bifurcation diagram is compared. The analysis predicts that the robust controller will shift the open loop bifurcation to the higher dynamic pressure. Increase of the dynamic pressure at the saddle-node bifurcation is a little bit smaller than the increase at the flutter point.

5 Wind Tunnel Test Verification of Closed Loop Bifurcation

5.1 Nominal Flutter Tests

Wind tunnel tests were planned and carried out at the transonic wind tunnel of JAXA in April 2005. Figure 8 and 9 show the wind model installed in the wind tunnel test section and the instrumentation diagram for the test, respectively. Since time has passed since the previous tests, confirmation tests of the nominal open loop flutter were first carried out. Several confirmation tests were carried out and typical time history of flutter is shown in Fig. 10. In this figure the acceleration at the #1 sensor point shows a sudden LCO in the upper chart with the wind tunnel pressure increasing in the second chart. The results are shown in Table 1.

Compared with the 1997 test flutter dynamic pressure of 27.9 kPa, every flutter in the table occurred lower dynamic pressure. Since we have repaired the model surface, the flutter characteristics have changed a bit. We chose 26.01 kPa of the fourth flutter as the new nominal flutter of the present 2005 test.

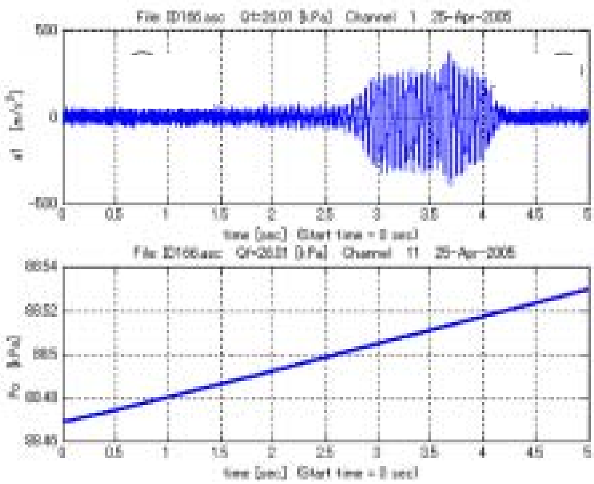

Fig. 10 Time history of accelerometer output and total pressure in wind tunnel

Table 1 Flutter point test results

No.	Dynamic Pressure [kPa]	LCO Amplitude [m]
1	25.85	0.01169
2	25.55	0.01128
3	25.13	0.01092
4	**26.01**	**0.01234**
5	25.83	0.01165

5.2 Excitation Tests above the Nominal Flutter Dynamic Pressure

Closed loop flutter tests were carried out in such a way that the robust controller CT03-161 was engaged at the wind tunnel pressure lower than the nominal flutter. The tunnel pressure was then increased until the closed loop flutter eventually occurred as shown in Fig. 11. Confirmed dynamic pressure of the closed loop flutter was 28.3 kPa.

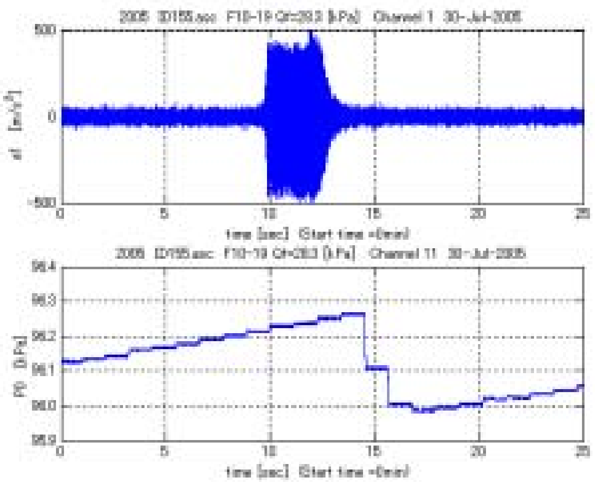

Fig. 11 Time history of flutter point test

We next executed excitation tests above the nominal flutter dynamic pressure. After engaging a control at a subcritical flutter dynamic pressure, we increased in quasi-static way the wind tunnel pressure above the nominal flutter at several different dynamic pressures. At each dynamic pressure, we applied a leading edge control surface a sinusoidal oscillation

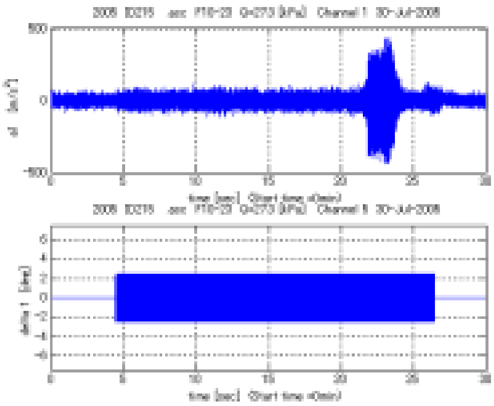

Fig. 12 Acceleration response of the wing caused by a leading edge surface excitation for a controlled flutter.

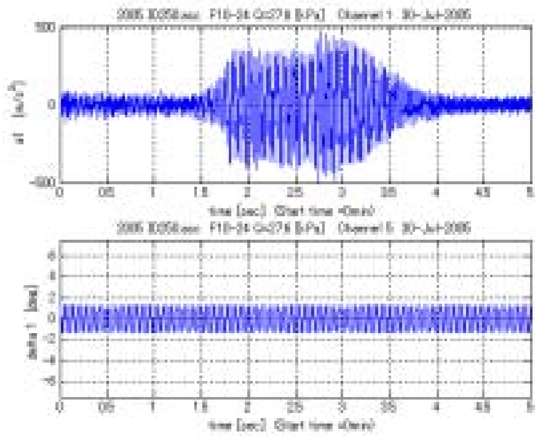

Fig. 13 Time history of LCO test (case: c)

with a frequency of 22.4 Hz, which is the flutter frequency. We increased amplitude of oscillation in stepwise way until the LCO occurred. Once LCO occurred, we stopped oscillation and observed whether LCO (or forced oscillation) will stop or continue. A typical response data obtained in the test is shown overall in Fig. 12 and in detail in Fig. 13. The upper chart in each figure shows an LCO at acceleration response caused by 2.5 deg amplitude sinusoidal excitation of a leading edge control surface. After confirming LCO, it is suppressed by operating a flutter-stopping device at the test section of the wind tunnel. Figure 14 summarizes these test results.

Integrating the acceleration data in LCO, we can depict the LCO amplitude in bifurcation diagram. Figure 15 shows the bifurcation diagram for the closed loop system along with a

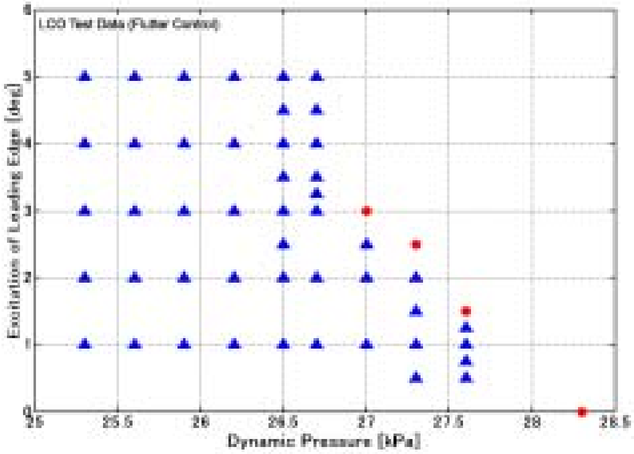

Fig. 14 LCO (flutter control) test result

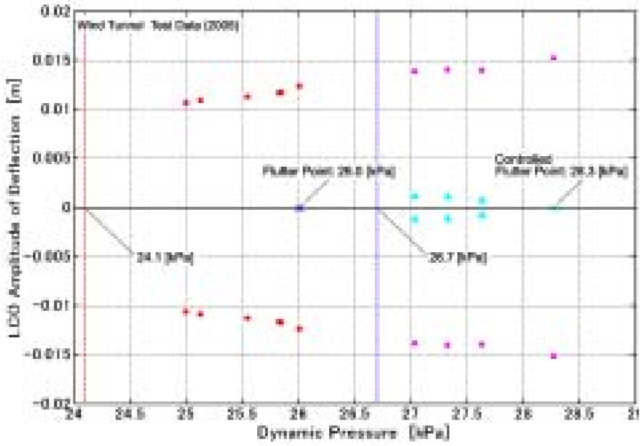

Fig. 15 Bifurcation diagram of 2005 wind tunnel test

open loop system. In case of controlled system, LCO is suppressed completely below the dynamic pressure 26.7 kPa. Three pairs of triangular points show just outside a separatrix, i. e., unsteady limit cycle.

5.3 Confirmation of the Predicted Bifurcation by the Wind Tunnel Tests

Adjusting free parameters in the mathematical model, we have renovated the model so as to fit the present wind tunnel test data. Resulting bifurcation diagram finally obtained is depicted in Fig. 16. Three sets of wind tunnel test data are just lying on the analytical LCO curve.

Based on the mathematical model closed loop bifurcation can be predicted as shown in Fig. 5.8. The figure shows the wind tunnel test data and it is clear that the analytical results predict surprisingly well the test data.

Figure 5-8 shows that the predicted bifurcation diagram for a closed loop system of flutter control can fundamentally be confirmed by the wind tunnel experiment.

6 Conclusions

The wind tunnel test was carried out with great care and limited numbers of LCO data at dynamic pressures above the open loop flutter point were successfully obtained. After confirming a flutter dynamic pressure of the controlled wing, we tried to excite the wing by a leading edge control surface oscillation at three different dynamic pressures in between the open and the closed loop flutter dynamic pressure.

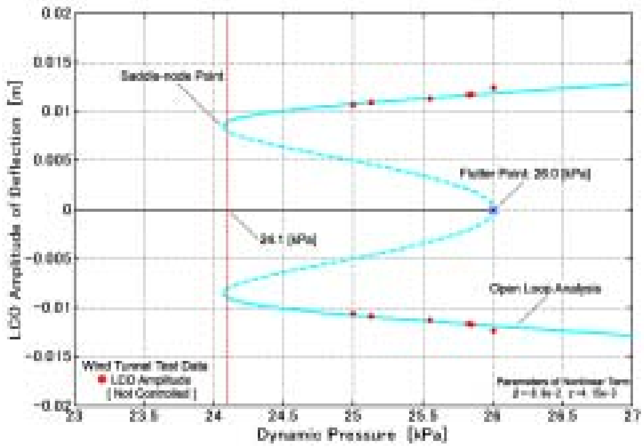

Fig. 5-7 Parameter adjusting on the bifurcation diagram, β=-8.9e-2, γ=4.15e-3

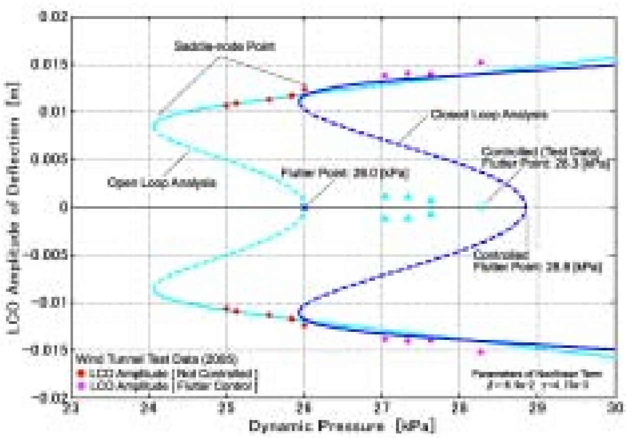

Fig. 5-8 Open loop and closed loop bifurcation diagram compared with 2005 test data

Even though the control might have lost the effectiveness due to large amplitude of LCO and resulting amplitude might have broken the wing seriously, we have succeeded in getting smaller amplitude of LCO.

Based on the mathematical model that was tuned to fit the new wind tunnel tests, the closed loop bifurcation for a robust controller used in the wind tunnel test was predicted. LCOs that were obtained in the tests have fitted well with the predicted LCO of the bifurcation diagram. Dynamic pressure of controlled flutter could be predicted in good coincident with the one obtained in the wind tunnel test as well.

References

[1] Cunningham A. M. Jr. Practical problem: airplanes. Chapter 3, *Unsteady transonic aerodynamics*, Nixon, D., ed., Progress in Astronautics and Aeronautics, 120, AIAA, pp 75-132, 1989.

[2] Dowell E H. Nonlinear Aeroelasticity. *Flight-Vehicle Materials, Structures and Dynamics*, 5, Part Ⅱ, Chapter 4, ASME, pp 213 – 239, 1993.

[3] Schewe G and Deyhle H. Experiments on transonic flutter of a two-dimensional supercritical wing with emphasis on the non-linear effects. *Proceedings of the Royal Aeronautical Society Conference on “UNSTEADY AERODYNAMICS”*, 1996.

[4] Matsushita H, Miyata T, Christiansen L E, Lehn-Schiøler T and Mosekilde E. On the Nonlinear Dynamics Approach of Modeling the Bifurcation for Transonic Limit Cycle Flutter, *Proceedings of the 24th International Congress of the Aeronautical Sciences*, pp 414.1 - 414.8, 2002.

[5] Isogai K. On the Transonic-Dip Mechanism of Flutter of a Sweptback Wing, *AIAA Journal*, Vol. 17, No. 7, pp 793-795.

[6] Saitoh K, Baldelli D H, Matsushita H, and Hashidate M. Robust controller design and its experimental validation for active transonic flutter suppression. *Proceedings of CEAS International Forum on Aeroelasticity and Structural Dynamics 1997*, Vol. II, Rome, 1997, pp 393-399.

[7] Matsushita H, Miyata T and Fujimori A. Possible Decrease in LCO Flutter Dynamic Pressure due to Robust Controller. *Proceedings of the 25th International Congress of the Aeronautical Sciences*, pp 5.10.3.1 - 8, 2004.

[8] Matsushita H, Saitoh K, and Gránásy P. Two degrees-of-freedom nonlinear math model with fourth order nonlinear aerodynamics for transonic limit cycle flutter. *CEAS/AIAA/ICASE/NASA LaRC International Forum on Aeroelasticity and Structural Dynamics 1999*, Williamsburg, US, June 1999.

[9] Matsushita H, Saitoh K, and Gránásy P. Nonlinear characteristics of transonic flutter of a high aspect ratio wing. *Proceedings of 21st ICAS*, Melbourne, pp 1-7, 1998.

[10] Hatta J. *Closed Loop Bifurcation for Control of Transonic Flutter and Its Wind Tunnel Test Verification*. Master Thesis, University of Fukui, Feb. 2006, in Japanese.

[11] Christiansen L E and Lehn-Schiøler T. Stochastic modeling of transonic flutter. Department of Physics, The Technical University of Denmark, Denmark, 2000.

[12] Christiansen L E, Lehn-Schiøler T, Mosekilde E, Gránásy P and Matsushita H. Nonlinear characteristics of randomly excited transonic flutter. *Mathematics and Computers in Simulation on Control of Oscillations and Chaos*, Vol. 58, pp 385 – 405, 2002.

[13] Mcfarlen D C and Glover K. *Robust Controller Design Using Normalized Coprime Factor Plant Descriptions*. Springer-Verlag, 1990.

[14] Fujimori A, Matsushita H, and Saitoh K. Model Modification of Transonic Aerodynamic Force on a High Aspect Ratio Aeroelastic Wing and Its Active Flutter Supression. *Proceedings of the 23rd International Congress of the Aeronautical Sciences,* Harrogate, UK, 2000.

[15] Baldelli D H, Matsushita H, Hashidate M, Saitoh K, and Ohta H. Flutter Margin Augmentation Synthesis Using Normarized Coprime Factors Approach. Journal of Guidance, Control and Dynamics, Vol. 18, No. 4, pp 803 – 811, 1995.

[16] Matsushita H, Saitoh K, and Gránásy P. Nonlinear characteristics of transonic flutter of a high aspect ratio wing. *Proceedings of 21st ICAS*, Melbourne, pp 1-7, 1998.